



UNIVERSITY OF LEEDS

This is a repository copy of *Correlation of bandgap reduction with inversion response in (Si)GeSn/high-k/metal stacks.*

White Rose Research Online URL for this paper:
<http://eprints.whiterose.ac.uk/113232/>

Version: Accepted Version

Article:

Schulte-Braucks, C, Narimani, K, Glass, S et al. (7 more authors) (2017) Correlation of bandgap reduction with inversion response in (Si)GeSn/high-k/metal stacks. *ACS Applied Materials and Interfaces*, 9 (10). pp. 9102-9109. ISSN 1944-8244

<https://doi.org/10.1021/acsami.6b15279>

© 2017 American Chemical Society. This document is the Accepted Manuscript version of a Published Work that appeared in final form in *ACS Applied Materials and Interfaces*, copyright © American Chemical Society after peer review and technical editing by the publisher. To access the final edited and published work see <https://doi.org/10.1021/acsami.6b15279>. Uploaded in accordance with the publisher's self-archiving policy.

Reuse

Unless indicated otherwise, fulltext items are protected by copyright with all rights reserved. The copyright exception in section 29 of the Copyright, Designs and Patents Act 1988 allows the making of a single copy solely for the purpose of non-commercial research or private study within the limits of fair dealing. The publisher or other rights-holder may allow further reproduction and re-use of this version - refer to the White Rose Research Online record for this item. Where records identify the publisher as the copyright holder, users can verify any specific terms of use on the publisher's website.

Takedown

If you consider content in White Rose Research Online to be in breach of UK law, please notify us by emailing eprints@whiterose.ac.uk including the URL of the record and the reason for the withdrawal request.



eprints@whiterose.ac.uk
<https://eprints.whiterose.ac.uk/>

Correlation of bandgap reduction with inversion response in (Si)GeSn/high-k/metal stacks

^{*1}C.Schulte-Braucks, ¹K. Narimani, ¹S. Glass, ¹N. von den Driesch, ²J.M. Hartmann, ³Z. Ikonic, ⁴V. V Afanas'ev, ¹Q.T. Zhao, ¹S. Mantl and ¹D. Buca

¹Peter Grünberg Institute 9 (PGI 9) and JARA-FIT, Forschungszentrum Juelich GmbH, 52425 Juelich, Germany

²Univ. Grenoble Alpes, 38000 Grenoble, France and CEA, LETI, Minatec Campus, 38054 Grenoble, France

³Institute of Microwaves and Photonics, Schools of Electronic and Electrical Engineering, University of Leeds, Leeds L2 9JT, United Kingdom

⁴Semiconductor Physics Laboratory, KU Leuven, 3001 Leuven, Belgium

Keywords: GeSn, high-k/metal gate, direct band gap, defects, generation/recombination.

*Corresponding author: c.schulte-braucks@fz-juelich.de

Abstract

The bandgap tunability of (Si)GeSn group IV semiconductors opens a new era in Si-technology. Depending on the Si/Sn contents, direct and indirect bandgaps in the range of 0.4 eV to 0.8 eV can be obtained, offering a broad spectrum of both photonic and low power electronic applications. In this work, we systematically studied capacitance-voltage characteristics of high-k/metal gate stacks formed on GeSn and SiGeSn alloys with Sn-contents ranging from 0 to 14 at.% and Si-contents from 0 to 10 at.% particularly focusing on the minority carrier inversion response. A clear correlation between the Sn-induced shrinkage of the bandgap energy and enhanced minority carrier response was confirmed using temperature and frequency dependent capacitance voltage-measurements, in good agreement with k.p theory predictions and photoluminescence measurements of the analyzed epilayers as reported earlier. The enhanced minority generation rate for higher Sn-contents can be firmly linked to the bandgap reduction in the GeSn epilayer without significant influence of substrate/interface effects. It thus offers a unique possibility to analyze intrinsic defects in (Si)GeSn epilayers. The extracted dominant defect level for minority carrier inversion lies approximately 0.4 eV above the valence band edge in the studied Sn-content range (0 to 12.5 at.%). This finding is of critical importance since it shows that the presence of Sn by itself does not impair the minority carrier lifetime. Therefore, the continuous improvement of (Si)GeSn material quality should yield longer non-radiative recombination times which are required for the fabrication of efficient light detectors and to obtain room temperature lasing action.

I. Introduction

Novel group IV alloys such as GeSn and SiGeSn pave a new path in Si-technology¹. The (Si)GeSn material system offers great flexibility in terms of band structure and strain engineering. The low direct bandgap of high-Sn content alloys makes them interesting for photonic applications² and for low-power electronic devices such as Tunneling Field Effect Transistors^{3,4}.

Furthermore, the low effective masses of Γ -electrons and holes together with the predicted high carrier mobility qualifies GeSn as an interesting alternative channel material⁵. Bandgap tuning of GeSn alloys has already been experimentally confirmed by photoluminescence measurements⁶ and lasing analysis^{2,7}. In this work, we present a systematic study of the influence of Sn-content on the electrical properties of high-k / metal gate stacks on GeSn and SiGeSn, namely on the capacitance voltage (CV) and conductance voltage (GV) characteristics.

The transition frequency of (Si)GeSn MOS structures, which is a measure of the minority carrier generation rate in (Si)GeSn, was extracted from CV measurements and compared for different Sn-contents up to 14 at.%. A clear trend of a continuously increasing minority carrier response with increasing Sn-content was observed, which went hand in hand with the band gap shrinkage expected when introducing more and more Sn into the alloy. On the other hand, the incorporation of Si in ternary SiGeSn alloys led to an increase of the bandgap which immediately reflected in the inversion response. Supported by TCAD device simulations of GeSn metal oxide semiconductor capacitors (MOSCaps), we show that these trends in inversion response are directly linked to the variations of the band gap and, therefore, represent an intrinsic property of the (Si)GeSn material system. Finally, using the temperature dependence of the inversion response, we extracted the energy of defect states (in the bandgap) which controlled the generation of minority carriers (electrons in the studied case) in the GeSn epilayers.

II. Experimental

Single crystalline GeSn and SiGeSn layers were grown epitaxially on 200 mm Ge-buffered Si(001) wafers (so called Ge-virtual substrate (GeVS)) by reduced pressure chemical vapor deposition (RPCVD⁸) at temperatures between 300 and 400°C. The Si-substrates are undoped with p-type carrier concentrations of low 10^{15} 1/cm³. Both GeVS and GeSn epilayers are undoped with p-type carrier concentrations ranging 10^{16} to 10^{17} 1/cm³ depending on the Sn-content. The

unintentional acceptor concentration in GeSn is presumably due to vacancies such as point defects in this compressively strained layers and increases with Sn-content^{9,10}. Details regarding growth have been reported elsewhere^{8,11}. After sample cleaning with organic solvents, oxygen plasma and HF-HCl wet chemistry, the (Si)GeSn samples were loaded into an atomic layer deposition tool where 6 nm thick HfO₂ layers were deposited at T=300°C using tetrakis ethylmethylamino hafnium (TEMAH), Hf[N(CH₃)(C₂H₅)]₄ and Ozone precursors. Subsequently, 60 nm thick TiN metal-gate was deposited by reactive RF-sputtering. In order to pattern the TiN, Al-contact pads were fabricated via lift-off. These Al-pads also served as a hard mask in the subsequent TiN metal gate patterning in a Cl₂:SF₆:Ar based reactive ion etching plasma. For the (Si)GeSn sample series in section IIB, Pt evaporated through a shadow mask was used as metal gate. The fabrication was finished by a forming gas anneal at 300°C for 10 min. Further details on the sample pre-cleaning and interface characterization of HfO₂/(Si)GeSn MOSCaps can be found in previous studies^{12,13}.

In order to analyze the influence of the bandgap on the CV-characteristics of (Si)GeSn based MOSCaps, a series of six samples with Sn-contents increasing from 0 up to 12.5 at.% were grown by RPCVD. The bandgaps of these semiconductor alloys are determined by the Sn-content and the residual compressive strain in the partially strain-relaxed layers. The bandgaps were calculated by including the alloy bowing factors, deformation potentials, and (at Γ) the eight-band k.p theory, using the Sn-content and strain coming from Rutherford Backscattering Spectrometry and X-Ray Diffraction reciprocal space mapping. An overview of the analyzed GeSn-samples is given in Table I and Fig. 1. Starting from 0.65 eV for Ge-VS (Ge is slightly tensile strained, +0.15%), the bandgap is reduced to 0.453 eV for Ge_{0.875}Sn_{0.125}. Relaxed GeSn undergoes a transition from an indirect to a direct semiconductor at a Sn content of about 8-9 at.%¹⁴. Consequently, the lower three Sn-content samples have an indirect bandgap whereas the higher three Sn-content samples

are fundamental direct bandgap semiconductors. The energies of the two lowest conduction band minima, Γ and L with respect to the highest hole band (Γ -point) are plotted in Fig. 1 for the range of Sn-contents analyzed here.

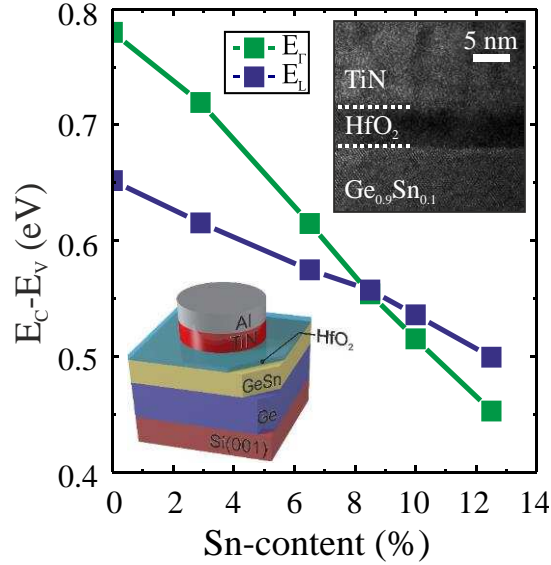


Fig.1: Direct and indirect bandgap energies of the different GeSn alloys analyzed in this study as functions of Sn-content. The samples with ≥ 8.5 at. % Sn are direct bandgap semiconductors. The lower left inset schematically illustrated the investigated layer stack. The upper right picture shows a Transmission Electron Micrograph indicating a smooth GeSn/HfO₂ interface.

Table I: Sn-content X_{Sn} , active layer thickness d , biaxial strain ϵ_{xx} , band gap E_g and conduction band minimum E_{cmin} of the GeSn samples analyzed here. The bandgap is calculated by including the alloy bowing factors, deformation potentials, and (at Γ) $k.p$ theory, using the measured strain values and Sn-concentrations. The first three samples are fundamental indirect while the latter three are fundamental direct bandgap semiconductors.

X_{Sn} (at. %)	d (nm)	ϵ_{xx} (%)	E_g (eV)	E_{cmin}
0	2500	0.15	0.652	L
2.9	51	-0.3	0.615	L
6.3	265	-0.31	0.575	L

8.5	768	-0.15	0.540	Γ
10	835	-0.27	0.515	Γ
12.5	414	-0.43	0.453	Γ

A. Electrical characterization

The fabricated MOSCaps were characterized by room temperature and temperature dependent multi-frequency CV-measurements in a frequency range from $f=1$ kHz to 1 MHz. In order to exclude the impact of series resistance on CV-characteristics a correction of the measured capacitance C_m and parallel conductance G_m has been applied, as proposed by Nichollian and Brews¹⁵:

$$C_c = \frac{(G_m^2 + \omega^2 C_m^2) C_m}{a^2 + \omega^2 C_m^2} \text{ and } G_c = \frac{(G_m^2 + \omega^2 C_m^2) a}{a^2 + \omega^2 C_m^2},$$

$$\text{where } a = G_m - (G_m^2 + \omega^2 C_m^2) R_s \text{ and } R_s = \frac{G_{ma}}{G_{ma}^2 + \omega^2 C_{ma}^2}.$$

C_c and G_c denote the corrected capacitance and conductance, and $\omega=2\pi f$. C_{ma} and G_{ma} are measured in strong accumulation. An overview of the CV-characteristics of the analyzed samples is presented in Fig. 2. All samples feature low dispersion in accumulation (here negative bias voltages) and small frequency-dependent flat band voltage shift, indicating good interface quality with the high-k dielectrics. This is supported by measurements of the interface trap densities, with a D_{it} of about $2 \times 10^{12} \text{ cm}^{-2} \text{ eV}^{-1}$, in agreement with literature reports^{12,16-18}. For voltages between -0.5 V and 0 V the so-called weak inversion hump appears, pointing towards an enhanced interaction of traps with both conduction and valence bands. However this hump is not a sign of a high D_{it} but is a characteristic of low band gap semiconductor MOSCaps¹⁹. The accumulation capacitance (negative bias) slightly decreases for increasing Sn-content indicating the formation of a GeSnO_x interlayer which will be suspect to future studies.

Furthermore it is evident that incorporation of Sn leads to an increase of the minority carrier response for these intrinsic p-type layers as seen from the CV behavior at positive voltages. This becomes obvious by comparing, for instance, the 200 kHz curves (pink curve) of the investigated capacitors as plotted in Fig. 2(g).

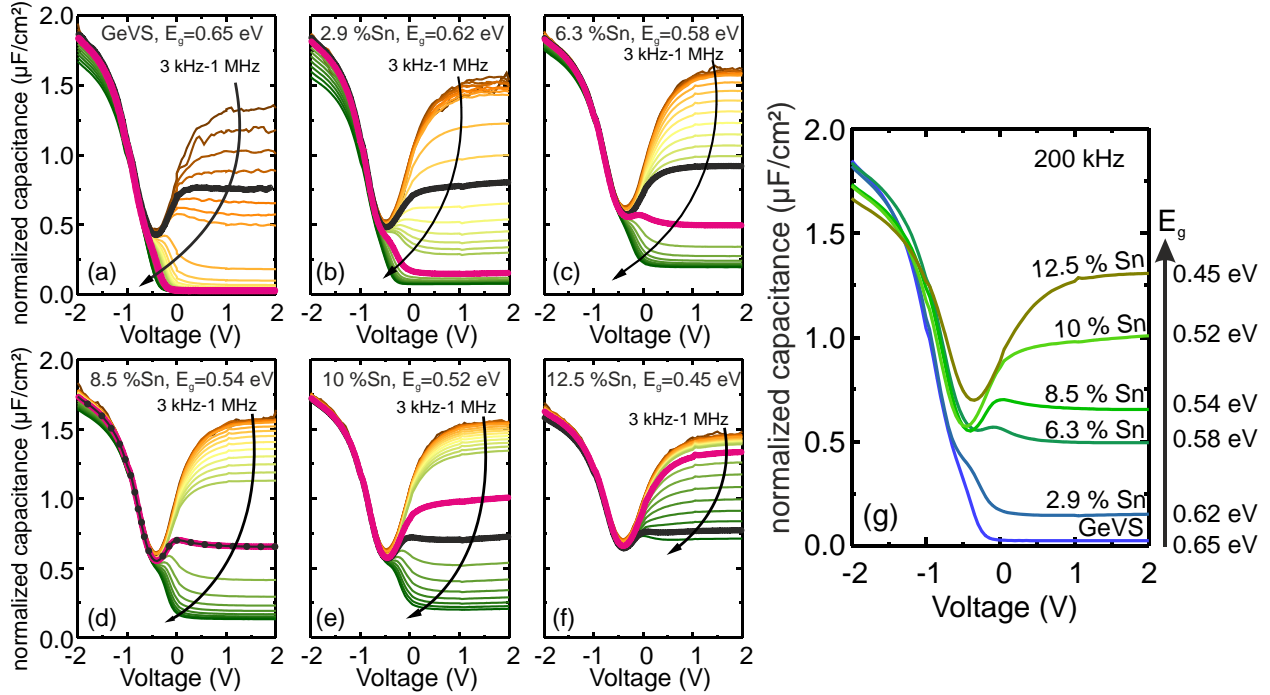


Fig. 2: (a-f), Examples of multi-frequency CV-traces of MOSCaps fabricated using different GeSn alloys. The reduced bandgap for higher Sn content alloys is reflected in an increased minority carrier response as seen from the 200 kHz curve (in pink). The black curves correspond to CV-characteristics measured at the transition frequency f_t . (g) Comparison of 200 kHz CV-characteristics for different GeSn alloy compositions taken from the measurements in (a-f).

In order to quantify the frequency behavior of the inversion response we define the transition frequency, f_t as the frequency where the measured capacitance is at midway between the low frequency capacitance C_{LF} and the high-frequency capacitance C_{HF} i.e. $C=0.5(C_{LF}+C_{HF})$. It has been shown in Refs. ⁽¹⁵⁾ and ⁽²⁰⁾ that, in strong inversion (here $V=+2$ V), the parallel conductance

divided by the angular frequency $G_p/\omega = G_p/(2\pi f)$ features a local maximum at the transition frequency and, thereby, provides an easy and accurate method to determine f_t . Several G_p/ω vs f curves taken at +2 V are shown in the inset of Fig. 3. The transition frequency vs. Sn-content dependence extracted as described is shown in Fig. 3. A lucid exponential increase of the transition frequency with increasing Sn-content i.e. with decreasing bandgap width is clearly visible.

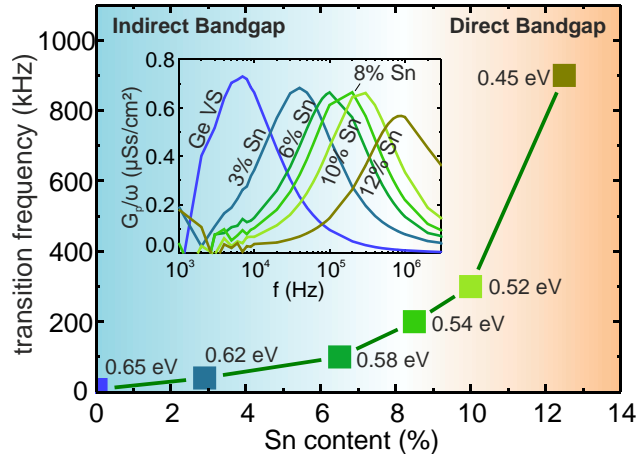


Fig. 3: Measured transition frequency vs. Sn-content showing a significant increase of f_t with increasing Sn-content i.e. decreasing bandgap. The inset depicts the corresponding G_p/ω vs. f curves measured in strong inversion (+2 V).

At this point two questions should be addressed: *i)* Can the enhanced minority carrier response with increased Sn-content be attributed solely to the bandgap decrease or, is it related to an increase of defect density in the GeSn epi-layer and/or GeSn/HfO₂ interface trap density D_{it} ?; *ii)* Is the physical mechanism responsible for the inversion response related to the generation/recombination or diffusion of the minority carriers?

Answers will be coming from CV-analysis of ternary SiGeSn MOSCaps and TCAD device simulations described in the next section. Simulations will also address the influence of the indirect-to direct band gap transition occurring when going to Sn-contents ≥ 8.5 at.%. Sn.

B. Inversion response in ternary SiGeSn MOSCaps

The incorporation of Si in binary GeSn alloys strongly modifies the electronic band structure. Whereas the incorporation of Sn leads to a band gap reduction compared to Ge, the incorporation of Si has the opposite effect²¹. That way, one can, for instance, obtain ternaries with a higher Sn-content than a corresponding GeSn-binary but with the same bandgap. By doing so one can decouple the effects originating from changes in the bandgap from those related to the material quality (e.g. defect concentration) when going to higher Sn-contents.

Fig. 4 shows the changes in the CV-characteristics for two series of (Si)GeSn MOSCaps. First, the Si-content was kept constant at about 5 at.% and the Sn-content was varied from 5 to 14 at.% (Fig. 4(a-c)). Second, the Sn-content was kept constant at about 10 at.% while the Si-content was changed from 0 to 10 at.% (Fig.4(c-e)). In a similar fashion to GeSn binaries, changes in bandgap are reflected in the minority carrier response: Increasing Sn-content leads to a bandgap shrinkage together with an enhanced minority carrier response. On the other hand, increasing Si-contents yield higher bandgaps, with a reduced minority carrier response, as seen for the 500 kHz curves in Fig.5(a,c). Quantitatively, these trends can be followed by monitoring the transition frequency of the different MOSCaps as plotted in Fig. 5(b,d).

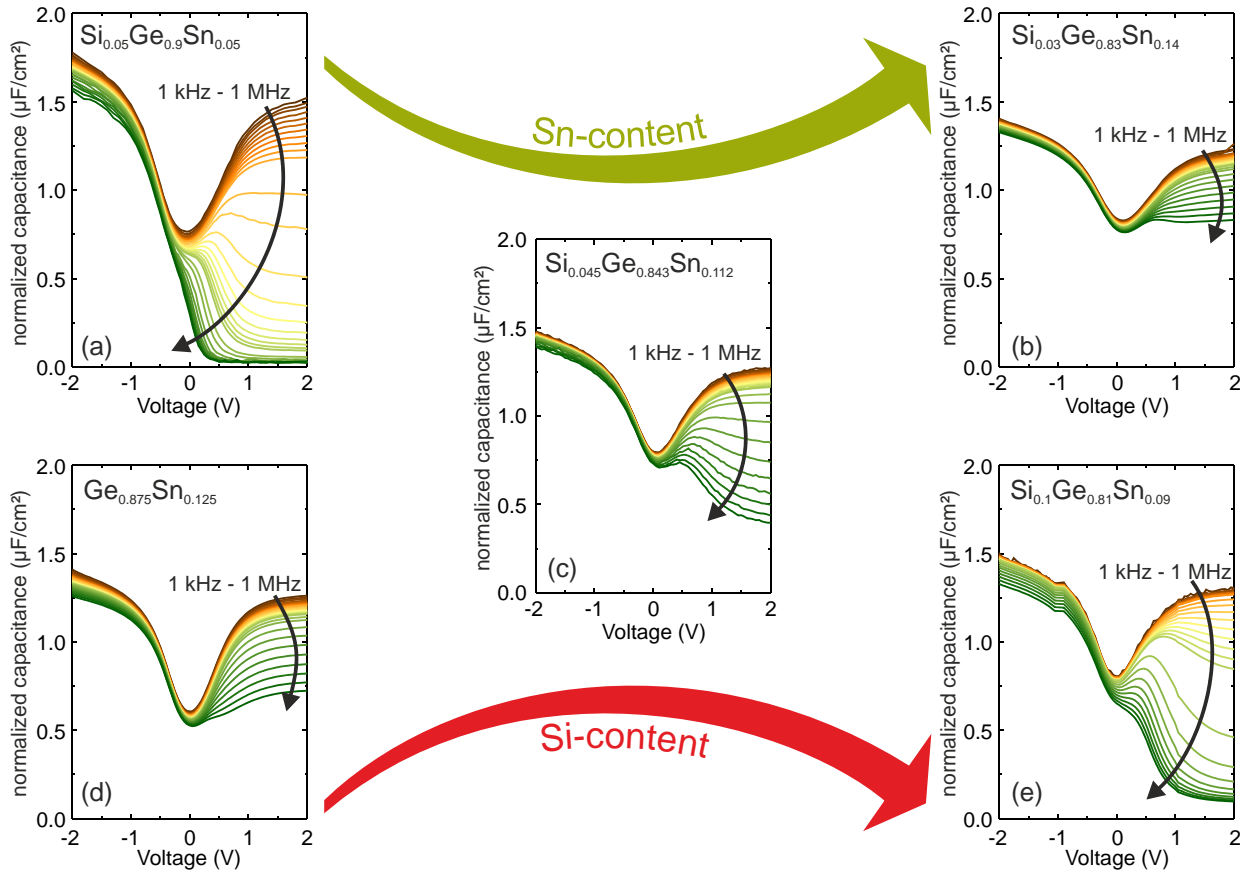


Fig. 4: Trends in the CV curve evolution in SiGeSn MOSCaps: The incorporation of Sn leads to an enhanced minority carrier response whereas the incorporation of Si leads to a reduction of the minority carrier response.

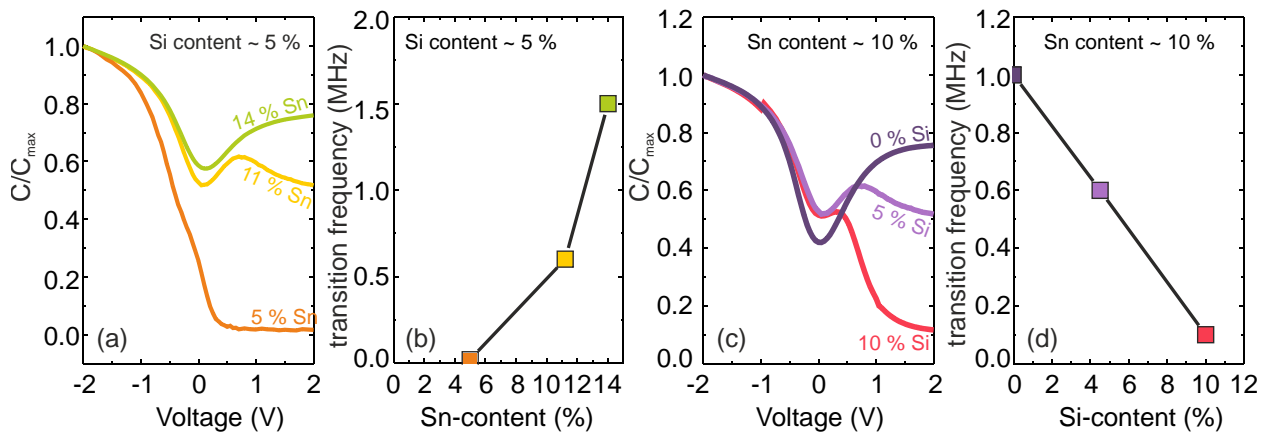


Fig. 5: 500 kHz curve and transition frequency for MOSCaps with different Si and Sn contents.

In the following discussion we will compare the inversion response of SiGeSn ternaries with those of GeSn binaries (in Fig. 3). The GeSn MOSCap with a Sn-content of 6.3 at.% shows a transition frequency of 100 kHz, whereas the $\text{Si}_{0.5}\text{Ge}_{0.9}\text{Sn}_{0.05}$ MOSCap with 5 at.% Si and 5 at.% Sn has a transition frequency of only 9 kHz. If the observed trends in transition frequency are dominated by differences in the substrate doping or bulk/interface defects induced by the Sn-content, similarly high transition frequencies can be expected for $\text{Si}_{0.05}\text{Ge}_{0.9}\text{Sn}_{0.05}$ and for $\text{Ge}_{0.937}\text{Sn}_{0.063}$ samples. Table II summarizes the measured transition frequencies for different SiGeSn and GeSn MOSCaps. The calculated bandgap of $\text{Si}_{0.05}\text{Ge}_{0.9}\text{Sn}_{0.05}$ corresponds to the one of GeVS and also the measured transition frequencies match well. Similarly for other Si and Sn content SiGeSn ternaries and their corresponding GeSn alloys, the transition frequencies are comparable, leading to the conclusion that the bandgap has the strongest influence on the inversion response. Also a possible change of the high-k/GeSn interface quality with increasing Sn-content can be excluded as the origin of the enhanced inversion response. Low temperature conductance measurements revealed a rather constant D_{it} over the whole investigated Sn-content range¹² and when biased to strong inversion, the interaction of interface traps with the conduction band is generally expected to be rather low^{15,22}.

However, the transition frequencies of comparable bandgap GeSn and SiGeSn alloys tend to differ somewhat, as the Si- and Sn-contents become really high. One can in turn conclude that material quality changes still can play a secondary role. Furthermore, the uncertainty in Si bowing parameters used for SiGeSn bandgap calculation might be an additional source of error.

To summarize, we conclude that the observed trends in the transition frequency as a function of Sn-content are essentially dominated by changes in the bandgap of the (Si)GeSn epilayer rather than by changes in material quality, interface quality or substrate background doping.

Table II: Calculated bandgap and measured transition frequencies of SiGeSn alloys compared to GeSn binaries having approximately the same bandgap.

SiGeSn alloy: (Si,Sn)-content (at. %)	E_g -calc (eV)	$f_{t-SiGeSn}$ (kHz)	Corresponding (Ge)Sn alloy	f_{t-GeSn} (kHz)
(5,5)	0.64	9	GeVS	7
(5,11)	0.54	500	GeSn (8.5 at.%)	200
(3,14)	0.51	1000	GeSn (10 at.%)	300

III. Device simulations

Device simulations have been performed using TCAD Sentaurus SDevice in order to substantiate the findings inferred from CV-measurements and to gain a deeper insight on the influence of band structure changes on the CV-characteristics of GeSn MOSCaps. Material input parameters for GeSn, i.e., band energies, bandgaps, effective masses, non-parabolicity coefficients etc. were calculated using the deformation potentials and k.p theory for the various Sn-content GeSn alloys taking into account the biaxial strain still present in the layers. For simplicity, and in order to focus on effects originating from changes of the band structure, no interface traps were assumed to affect the simulated MOSCap characteristics, since we are mainly interested in the inversion region, whereas the response of traps is dominant in depletion and weak inversion^{15,22}. For the calculation of Shockley-Read-Hall (SRH) generation/recombination, the presence of traps in the vicinity of the midgap was considered. It will be shown later on (see the Arrhenius analysis) that SRH is the dominant mechanism for minority carrier generation in inversion. Because of this, for simplicity, the diffusion parameters as well as mobilities were fixed to those of bulk Ge for all epitaxial layers.

Fig. 6(a) shows the calculated 200 kHz CV-characteristics of GeSn MOSCaps with different Sn-contents. The doping was set to $2 \times 10^{17} \text{ cm}^{-3}$, according to carrier concentrations measured by the

Electrochemical Capacitance Voltage (ECV) technique. The SRH-time is set to $\tau=500$ ps (in the range extracted by Wirths, Geiger *et al.*²). The good agreement with experimental data shown in Fig. 2(g) is obvious. Please note that the aim of our CV simulations was to provide a deeper understanding of the effects arising from changes in bandgap, doping, τ and direct vs. indirect bandgap, but not to precisely reproduce the experimental curves. With use of the physics based simulations, precise fitting of the CV and GV data might though be done in a future study since it would allow the extraction of minority carrier generation rates, as reported by Monaghan *et al.*²⁰. As the generation rate is closely related to the density of near mid gap traps this material parameter is of interest for both electronic and photonic application.

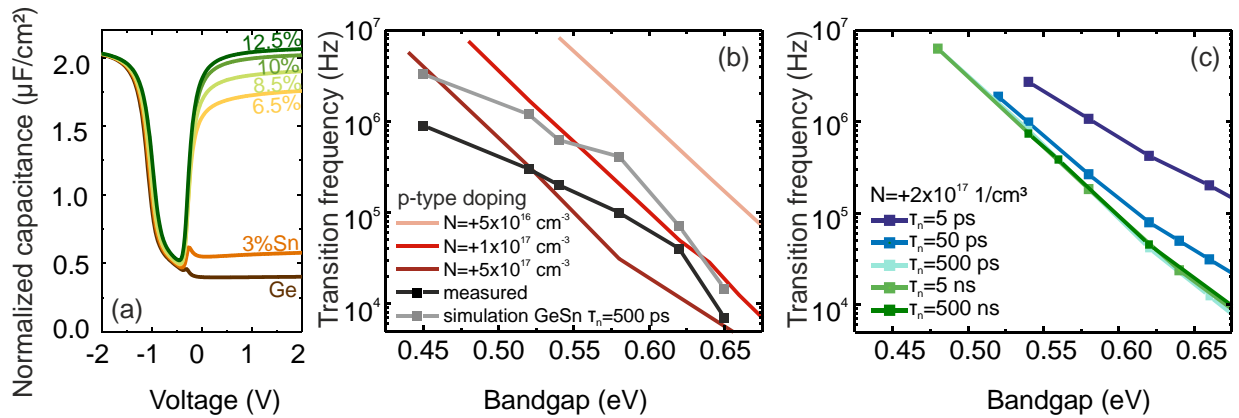


Fig. 6: (a) Simulated CV-curves at 200 kHz for MOSCaps with different GeSn alloys. (b) The transition frequency vs. bandgap width as measured and simulated for the GeSn layers and for Ge crystals using the Ge band structure with variable bandgap width for three different p-type doping levels. (c) Corresponding simulations of f_t as shown in panel (b) but with SRH constant τ_n as a parameter.

Let us first look at what happens when changing the bandgap value E_g only (e.g. when using the Ge-band structure and reducing E_g , while keeping the effective masses, the Γ -L-valley splitting

constant etc.). An exponential increase of the transition frequency is then expected, when reducing the bandgap¹⁵ following $\log(f_t) \sim -E_g/kT$, as shown in Fig. 6(b). Here, the red shaded curves show the transition frequency plotted versus E_g (with a Ge-like band structure) for three p-type doping concentrations N . The transition frequency increases with decreasing bandgap and decreasing doping. Changes in N lead to parallel lines in the f_t - E_g plot. Experimentally, the p-type background concentration in undoped GeSn increases with the Sn-content. In the Sn-content range analyzed here the acceptor concentration changes from the low 10^{16} cm^{-3} range for pure Ge up to the low 10^{17} cm^{-3} range for a 12.5 at.% GeSn alloy. Doping variations thus cannot explain the observed increase of f_t with the Sn-content. Higher Sn-contents would indeed yield higher carrier concentrations and thus lower f_t .

The third dependence of f_t that has to be considered is that on the minority carrier lifetime τ_n . This dependence is shown in Fig. 6(c). Shorter carrier lifetimes lead to an increase of f_t . It should, however, be pointed out that the dependence of f_t on τ_n is weaker than the dependence on E_g in the experimentally meaningful range. Even τ_n changes by several orders of magnitude, which would correspond to a significant increase of the defect density in the epi-layer when going towards higher Sn-contents, could not explain the observed changes in f_t .

Summarizing the influence of those factors (E_g , N , τ_n) on the transition frequency, we conclude that the experimentally observed increase of f_t with increasing Sn-content is mainly due to changes in the material bandgap. At the same time, higher carrier concentrations stemming from higher Sn-contents yield lower f_t . Since this dependence is opposing the trend of decreasing bandgap, the curve of the measured f_t -vs- E_g plot in Fig. 6(b) is flattened out for low E_g values compared to a “pure” bandgap trend. The grey curve in Fig. 6(b) shows simulated f_t vs E_g behavior for the different GeSn alloys with Sn-contents ranging from 0 to 12.5 at.% for a fixed doping

concentration of $2 \times 10^{17} \text{ cm}^{-3}$ and $\tau_n = 500 \text{ ps}$ taking into account their band-structures calculated by k.p theory (band energies, effective masses, non-parabolicities etc.). Interestingly, also the theoretical f_t -vs- E_g curve does not strictly obey a $\log(f_t) \sim E_g/k_B T$ law (despite the constant doping). It rather follows two trend lines, one for smaller and one for larger bandgaps. An additional factor one has to take into account when analyzing the f_t -vs- E_g plot for different Sn-contents is that not only the bandgap changes when going to higher Sn-contents. The alloy also undergoes a transition from an indirect to a fundamental direct semiconductor. Since Γ and L valleys have significantly different effective masses and density of states (DOS) we attribute the change in the slope of the f_t -vs- E_g curve to changes in the Fermi-level position originating from changes in the conduction band DOS as outlined by the simulation results shown in Fig 7. Here the plot shows f_t -vs- E_g for “regular” (i.e. indirect) Ge band structures with variable E_g and for “artificially” direct Ge where Γ and L energies are swapped. Again f_t continuously increases as the bandgap decreases. However, f_t for the direct bandgap case is significantly smaller due to the smaller DOS. The measured data are in between these two curves as GeSn undergoes the indirect to direct transition within the analyzed Sn-contents. Since momentum conservation does not apply for SRH, it should be pointed out that, for fixed τ_n here, the fact whether the material is direct or indirect only plays a role in terms of conduction band DOS via the effective mass differences. Also quantum confinement effects that might occur in the two dimensional inversion layer²³ especially for low DOS direct band gap GeSn do not affect the CV inversion response. This is seen in Fig. 2 and 4 where the frequency dispersion in inversion ($> +0.5 \text{ V}$) does only change slightly with increasing gate bias while the inversion charge density is increasing. Especially since the width of the quantized inversion region in semiconductor is small (a few nm) as compared to the width of the depletion layer ($> 100 \text{ nm}$), its contribution to the minority carrier generation rate is negligible.

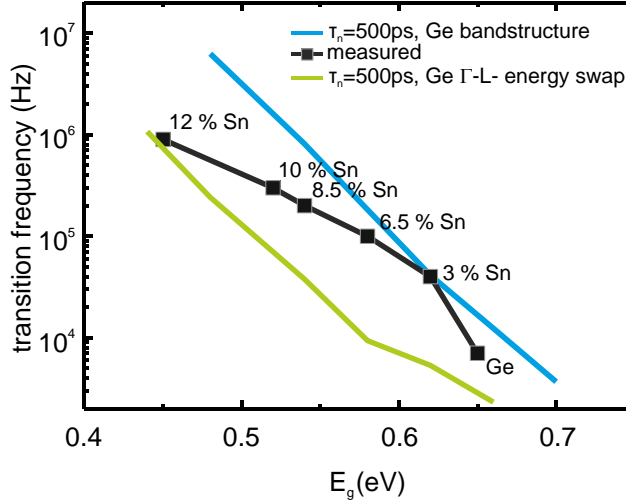


Fig. 7: Transition frequency vs. bandgap for (indirect) Ge band structure with variable E_g and for the “artificially direct” Ge band structure with Γ and L energies swapped. Since the GeSn layers undergo an indirect to direct transition within the analyzed Sn-content range, the experimentally measured curve appears between these extremes.

IV. Temperature Dependent CV and Conductance Measurements

In the previous sections it was shown that the observed trends in inversion response are directly linked to minority generation within the GeSn epilayer, providing unique opportunities to study intrinsic material defects whereas with other techniques such as Deep Level Transient Spectroscopy (DLTS), it is difficult to attribute the detected traps to a certain semiconductor layer.

For this purpose we performed temperature dependent CV-measurements in the range from 80 K to room temperature. Since the strong inversion response present at room temperature is created by generation/recombination (see the Arrhenius analysis below), it can be effectively suppressed when lowering the sample temperature. This can be seen in the CV-behavior in Fig. 8. In turn, the conductance signal in inversion, stemming from SRH generation/recombination at room temperature is also suppressed at low temperature as can be seen in Fig. 9 showing the

conductance-frequency maps for MOSCaps fabricated on Ge and on $\text{Ge}_{0.9}\text{Sn}_{0.1}$. At the same time, the behavior of majority carriers (accumulation) is seen to be insignificantly affected by the variation of temperature.

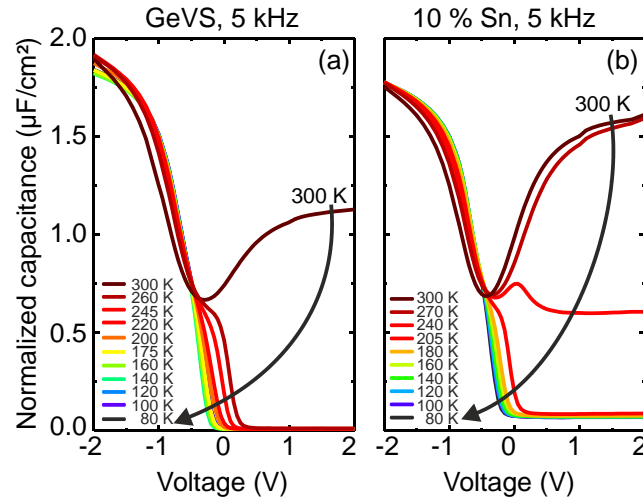


Fig. 8: CV characteristics at 5 kHz for different temperatures in the 80-300 K range for GeVS and $\text{Ge}_{0.9}\text{Sn}_{0.1}$ demonstrating the reduced inversion response at low temperature.

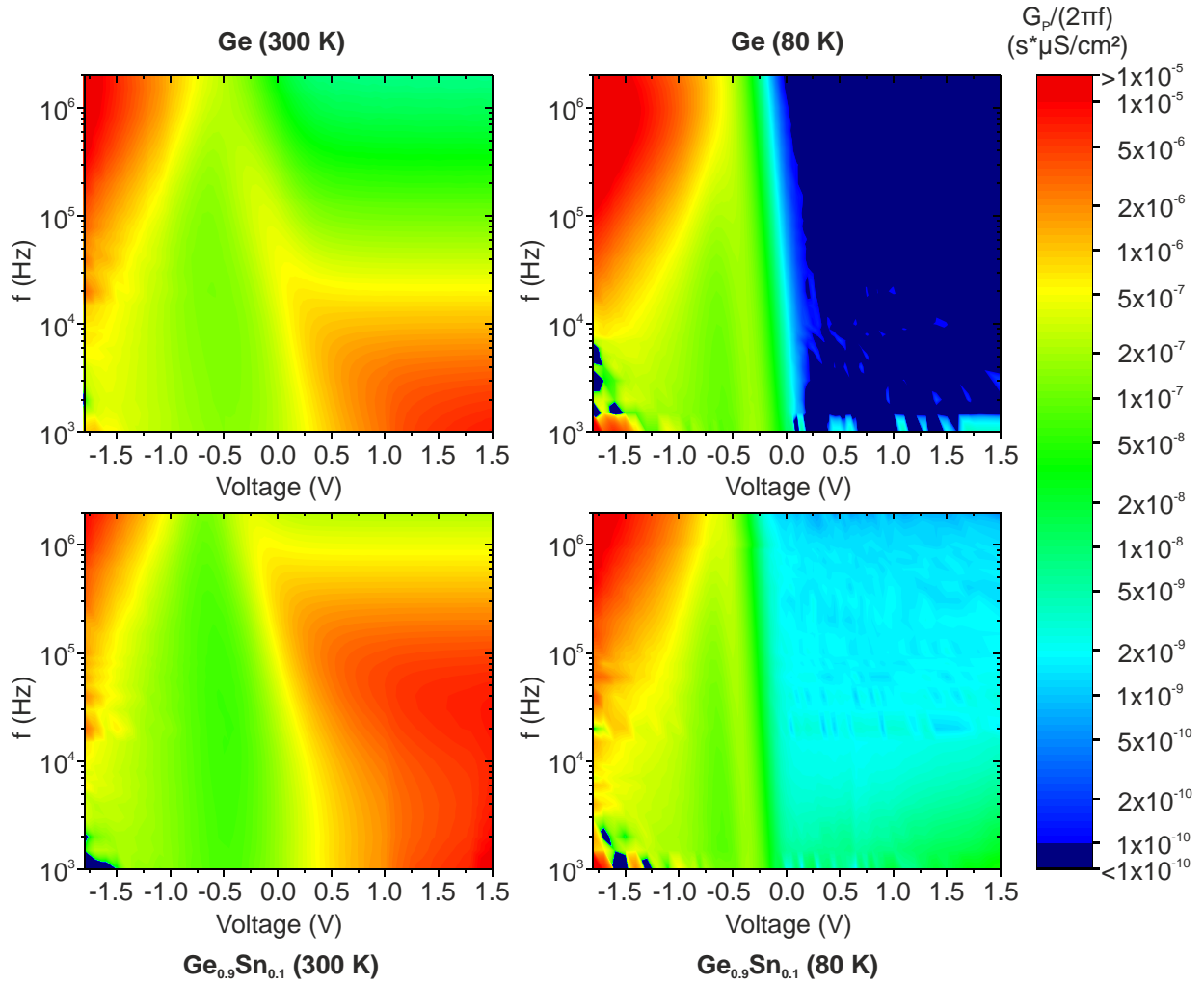


Fig 9: Parallel conductance G_p/ω for Ge (top) and $Ge_{0.9}Sn_{0.1}$ (bottom) MOSCaps at room temperature (left) and at 80 K (right). The conductance in inversion (which is generated by SRH) is suppressed at low temperature.

Arrhenius Analysis of the Conductance

The CV-behavior in inversion can be approximated by the equivalent circuit depicted in the inset of Fig. 10(a) where C_{ox} is the oxide capacitance, C_D the depletion capacitance and G_{gr} and G_d the generation/recombination and diffusion conductances, respectively. The inversion conductance $G_i = G_{gr} + G_d$ can be extracted from the measurement data as follows¹⁵:

$$G_i = \frac{\omega^2 C_{ox} \tau_0 (1 + \omega^2 \tau_m^2)}{\omega^2 \tau_0^2 + [\omega^2 \tau_m (\tau_0 - \tau_m) - 1]^2}, \text{ where } \tau_m = C_m / G_m \text{ and } \tau_0 = C_{ox} / G_m.$$

The temperature dependence of G_i reveals whether the inversion is dominated by generation recombination or by diffusion¹⁵. For diffusion dominated inversion, a linear fit of $\log(G_i)$ vs. $1/kT$ would yield activation energies $E_a \sim E_g$ whereas for generation/recombination dominated inversion $E_a \leq E_g/2$.

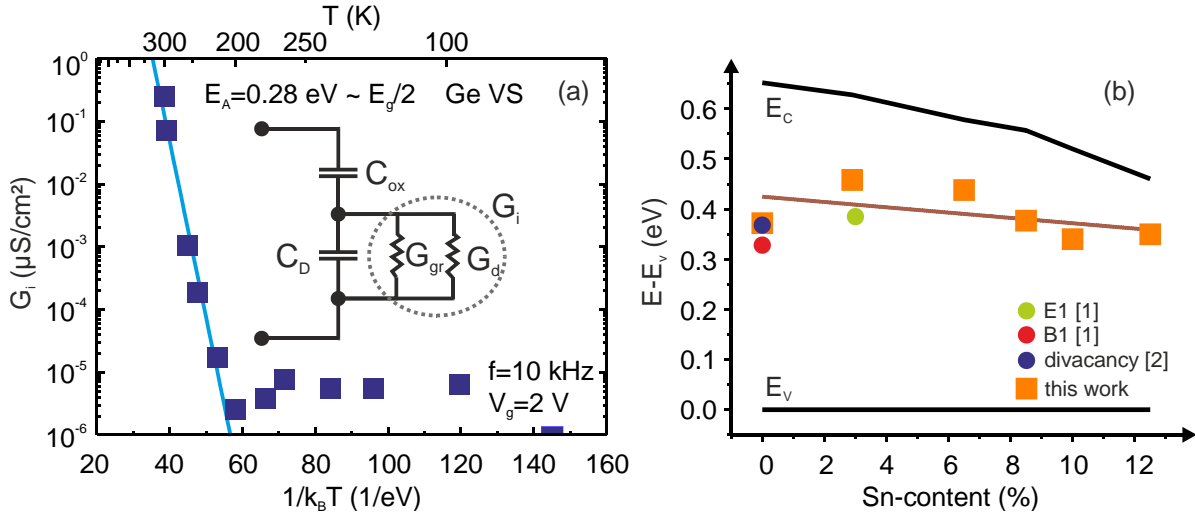


Fig. 10: (a) Arrhenius analysis of the intrinsic conductance G_i for Ge yields an activation energy of 0.28 eV. The equivalent circuit for the extraction of G_i in strong inversion (+2 V) is depicted in the inset. (b) Activation energies extracted from Arrhenius analysis for different Sn-contents referenced to the GeSn bandgap edges, together with deep defect levels known from literature: [1] Takeuchi et al.²⁴, [2] Fage-Pedersen et al.²⁵. The brown line is a linear fit of the data as a guide to the eye.

Table III: Activation energies for minority carrier generation extracted from Arrhenius analysis of conductance in strong inversion.

Sn-content (at. %)	E_a (eV)
0	0.28
2.9	0.17
6.3	0.14
8.5	0.18
10	0.18
12.5	0.11

The extracted activation energies E_a are shown in Table III. As all extracted activation energies are smaller than $E_g/2$ it can be concluded that, in strong inversion at room temperature, the CV-characteristics in the investigated Sn-content range are dominated by generation/recombination. Since this method reveals activation energies for the generation of electrons, these energies are measured relative to the conduction band and reside in the upper half of the bandgap. Increasing Sn-content mainly leads to a down-shift of the conduction band minimum E_c such that $E_t = E_c - E_a$ provides the position of the defect levels within the bandgap. As shown in Fig. 10(b), the extracted defect levels are rather constant at ~ 0.38 eV above the valence band energy E_v over the whole analyzed Sn-content range. Consequently, the enhanced inversion response for higher Sn-content (and thus lower bandgaps) can be explained by the downshift of the conduction band towards the trap level with increasing Sn-content. This result suggests that these defects are pertinent to the Ge sub-lattice (as they are also found in the Sn-free Ge reference sample), indicating that the incorporation of Sn is not the main source of this defect. A comparison with the literature shows good agreement with di-vacancy defect in Ge²⁵ ($E_t = E_c - 0.29 = E_v + 0.385$ eV) and the E2 peak reported for Ge_{0.968}Sn_{0.032} ($E_t = E_c - 0.23$ eV = $E_v + 0.38$ eV)²⁴. The fact that the dominant defects for generation/recombination observed here are not necessarily primarily Sn-related (e.g. a vacancy

complex) could be promising for further improvements in GeSn material quality since these defects may limit the non-radiative carrier lifetimes (SRH generation/recombination life times) needed for optoelectronic devices such as efficient photodetectors or lasers operating at room temperature.

V. Conclusions

To summarize we have presented a detailed Capacitance-Voltage (CV) study of (Si)GeSn Metal Oxide Semiconductor Capacitors. The evolution of the bandgap when changing the Sn-content is clearly reflected in the minority response of the CV-characteristics. Comparative analysis of samples fabricated using ternary SiGeSn alloys allowed us to decouple the trends arising from changes in the Sn-content and those coming from changes in the bandgap width. The experimental results were supported by k,p band structure and TCAD device simulations. A constant generation level at ~ 0.38 eV above the valence band independently of the Sn-content (up to 12.5 at.%) was evidenced by variable temperature CV measurements. As a further analysis the CV and GV measurements shown here in conjunction with the physics based ac-simulations could allow the determination of carrier generation lifetimes in the (Si)GeSn epitaxial layers which is of high relevance to both electronic and photonic application.

Acknowledgements

This research received funding from the EU FP7 Project E2SWITCH (619509) and the German Federal Ministry of Education and Research (BMBF) project UltraLowPow (16ES0060 K).

References

- (1) Wirths, S.; Buca, D.; Mantl, S. Si–Ge–Sn Alloys: From Growth to Applications. *Prog. Cryst. Growth Charact. Mater.* **2016**, *62* (1), 1–39.
- (2) Wirths, S.; Geiger, R.; von den Driesch, N.; Mussler, G.; Stoica, T.; Mantl, S.; Ikonic, Z.; Luysberg, M.; Chiussi, S.; Hartmann, J. M.; Sigg, H.; Faist, J.; Buca, D.; Grützmacher, D. Lasing in Direct-Bandgap GeSn Alloy Grown on Si. *Nat. Photonics* **2015**, *9* (2), 88–92.
- (3) Pandey, R.; Schulte-Braucks, C.; Sajjad, R. N.; Barth, M.; Ghosh, R. K.; Grisafe, B.; Sharma, P.; Driesch, N. von den; Vohra, A.; Rayner, B.; Mantl, S.; Buca, D.; Yeh, C.-C.; Wu, C.-H.; Tsai, W.; Antoniadis, D.; Datta, S. Performance Benchmarking of P-Type In_{0.65}Ga_{0.35}As/GaAs_{0.4}Sb_{0.6} and Ge/Ge_{0.93}Sn_{0.07} Hetero-Junction Tunnel FETs. In *2016 IEEE International Electron Devices Meeting (IEDM)*; 2016; pp 19.6.1–19.6.4.
- (4) Yang, Y.; Han, G.; Guo, P.; Wang, W.; Gong, X.; Wang, L.; Low, K. L.; Yeo, Y. Germanium-Tin P-Channel Tunneling Field-Effect Transistor: Device Design and Technology Demonstration. *IEEE Trans. Electron Devices* **2013**, *60* (12), 4048–4056.
- (5) Sau, J. D.; Cohen, M. L. Possibility of Increased Mobility in Ge-Sn Alloy System. *Phys. Rev. B* **2007**, *75* (4), 045208.
- (6) Stange, D.; Wirths, S.; von den Driesch, N.; Mussler, G.; Stoica, T.; Ikonic, Z.; Hartmann, J. M.; Mantl, S.; Grützmacher, D.; Buca, D. Optical Transitions in Direct-Bandgap Ge_{1-x}Sn_x Alloys. *ACS Photonics* **2015**, *2* (11), 1539–1545.
- (7) Stange, D.; Wirths, S.; Geiger, R.; Schulte-Braucks, C.; Marzban, B.; Driesch, N. V. Den; Mussler, G.; Zabel, T.; Stoica, T.; Hartmann, J.-M.; Mantl, S.; Ikonic, Z.; Grützmacher, D.; Sigg, H.; Witzens, J.; Buca, D. Optically Pumped GeSn Microdisk Lasers on Si. *ACS Photonics* **2016**, *3* (7), 1279–1285.
- (8) von den Driesch, N.; Stange, D.; Wirths, S.; Mussler, G.; Holländer, B.; Ikonic, Z.;

- Hartmann, J. M.; Stoica, T.; Mantl, S.; Grützmacher, D.; Buca, D. Direct Bandgap Group IV Epitaxy on Si for Laser Applications. *Chem. Mater.* **2015**, *27* (13), 4693–4702.
- (9) Nakatsuka, O.; Tsutsui, N.; Shimura, Y.; Takeuchi, S.; Sakai, A.; Zaima, S. Mobility Behavior of Ge 1- X Sn X Layers Grown on Silicon-on-Insulator Substrates. *Jpn. J. Appl. Phys.* **2010**, *49* (4), 04DA10.
- (10) Kamiyama, E.; Nakagawa, S.; Sueoka, K.; Ohmura, T.; Asano, T.; Nakatsuka, O.; Taoka, N.; Zaima, S.; Izunome, K.; Kashima, K. Effect of Sn Atoms on Incorporation of Vacancies in Epitaxial Ge 1- X Sn X Film Grown at Low Temperature. *Appl. Phys. Express* **2014**, *7* (2), 021302.
- (11) von den Driesch, N.; Stange, D.; Wirths, S.; Rainko, D.; Postugar, I.; Savenko, A.; Breuer, U.; Geiger, R.; Sigg, H.; Ikonic, Z.; Hartmann, J. M.; Grützmacher, D.; Mantl, S.; Buca, D. SiGeSn Ternaries for Efficient Group IV Heterostructure Light Emitters. *Small* **2017**, *in press*.
- (12) Schulte-Braucks, C.; von den Driesch, N.; Glass, S.; Tiedemann, A. T.; Breuer, U.; Besmehn, A.; Hartmann, J.-M.; Ikonic, Z.; Zhao, Q. T.; Mantl, S.; Buca, D. Low Temperature Deposition of High-k/Metal Gate Stacks on High-Sn Content (Si)GeSn-Alloys. *ACS Appl. Mater. Interfaces* **2016**, *8* (20), 13133–13139.
- (13) Wirths, S.; Stange, D.; Pampillón, M.-A.; Tiedemann, A. T.; Mussler, G.; Fox, A.; Breuer, U.; Baert, B.; San Andrés, E.; Nguyen, N. D.; Hartmann, J.-M.; Ikonic, Z.; Mantl, S.; Buca, D. High- K Gate Stacks on Low Bandgap Tensile Strained Ge and GeSn Alloys for Field-Effect Transistors. *ACS Appl. Mater. Interfaces* **2015**, *7* (1), 62–67.
- (14) Stange, D.; Wirths, S.; Geiger, R.; Schulte-Braucks, C.; Marzban, B.; Driesch, N. von den; Mussler, G.; Zabel, T.; Stoica, T.; Hartmann, J.-M.; Mantl, S.; Ikonic, Z.; Grützmacher, D.;

- Sigg, H.; Witzens, J.; Buca, D. Optically Pumped GeSn Microdisk Lasers on Si. *ACS Photonics* **2016**, *3* (7), 1279–1285.
- (15) Nicollian, E. H.; Brews, J. R. *MOS (Metal Oxide Semiconductor) Physics and Technology*; Wiley, 2002.
- (16) Gupta, S.; Simoen, E.; Loo, R.; Madia, O.; Lin, D.; Merckling, C.; Shimura, Y.; Conard, T.; Lauwaert, J.; Vrielinck, H.; Heyns, M. Density and Capture Cross-Section of Interface Traps in GeSnO₂ and GeO₂ Grown on Heteroepitaxial GeSn. *ACS Appl. Mater. Interfaces* **2016**, *8* (21), 13181–13186.
- (17) Gupta, S.; Chen, R.; Harris, J. S.; Saraswat, K. C. Atomic Layer Deposition of Al₂O₃ on Germanium-Tin (GeSn) and Impact of Wet Chemical Surface Pre-Treatment. *Appl. Phys. Lett.* **2013**, *103* (24), 241601.
- (18) Merckling, C.; Sun, X.; Shimura, Y.; Franquet, A.; Vincent, B.; Takeuchi, S.; Vandervorst, W.; Nakatsuka, O.; Zaima, S.; Loo, R.; Caymax, M. Molecular Beam Deposition of Al₂O₃ on P-Ge(001)/Ge_{0.95}Sn_{0.05} Heterostructure and Impact of a Ge-Cap Interfacial Layer. *Appl. Phys. Lett.* **2011**, *98* (19), 192110.
- (19) Martens, K.; Chui, C. O.; Brammertz, G.; De Jaeger, B.; Kuzum, D.; Meuris, M.; Heyns, M.; Krishnamohan, T.; Saraswat, K.; Maes, H. E.; Groeseneken, G. On the Correct Extraction of Interface Trap Density of MOS Devices With High-Mobility Semiconductor Substrates. *IEEE Trans. Electron Devices* **2008**, *55* (2), 547–556.
- (20) Monaghan, S.; O'Connor, E.; Rios, R.; Ferdousi, F.; Floyd, L.; Ryan, E.; Cherkaoui, K.; Povey, I. M.; Kuhn, K. J.; Hurley, P. K. Capacitance and Conductance for an MOS System in Inversion, with Oxide Capacitance and Minority Carrier Lifetime Extractions. *IEEE Trans. Electron Devices* **2014**, *61* (12), 4176–4185.

- (21) Attiaoui, A.; Moutanabbir, O. Indirect-to-Direct Band Gap Transition in Relaxed and Strained Ge_{1-x-y}Si_xSn_y Ternary Alloys. *J. Appl. Phys.* **2014**, *116* (6), 063712.
- (22) Batude, P.; Garros, X.; Clavelier, L.; Le Royer, C.; Hartmann, J. M.; Loup, V.; Besson, P.; Vandroux, L.; Campidelli, Y.; Deleonibus, S.; Boulanger, F. Insights on Fundamental Mechanisms Impacting Ge Metal Oxide Semiconductor Capacitors with High-K/metal Gate Stacks. *J. Appl. Phys.* **2007**, *102* (3), 034514.
- (23) Stern, F. Self-Consistent Results for N-Type Si Inversion Layers. *Phys. Rev. B* **1972**, *5* (12), 4891–4899.
- (24) Takeuchi, W.; Asano, T.; Inuzuka, Y.; Sakashita, M.; Nakatsuka, O.; Zaima, S. Characterization of Shallow- and Deep-Level Defects in Undoped Ge_{1-X}Sn_X Epitaxial Layers by Electrical Measurements. *ECS J. Solid State Sci. Technol.* **2016**, *5* (4), P3082–P3086.
- (25) Fage-Pedersen, J.; Larsen, A. N.; Mesli, A. Irradiation-Induced Defects in Ge Studied by Transient Spectroscopies. *Phys. Rev. B* **2000**, *62* (15), 10116–10125.

Table of Contents (TOC) graphic

